J. Fluid Mech. (1991), *vol.* 226, *pp.* 625–654
Printed in Great Britain

Boundary-driven mixing

By ANDREW W. WOODS†
Institute of Geophysics and Planetary Physics, Scripps Institution of Oceanography, La Jolla, CA 92093, USA

(Received 19 January 1990 and in revised form 29 November 1990)

There are two separate mechanisms which can generate a boundary flow in a non-rotating, stratified fluid. The Phillips–Wunsch boundary flow arises in a stratified, quiescent fluid along a sloping boundary. Isopycnals are deflected from the horizontal in order to satisfy the zero normal mass flux condition at the boundary; this produces a horizontal density gradient which drives a boundary flow. The second mechanism arises when there is an independently generated turbulent boundary layer at the wall such that the eddy diffusion coefficients decay away from the wall; if the vertical density gradient is non-uniform the greater eddy diffusion coefficients near the wall result in a greater accumulation or diminution of density near the wall. This produces a horizontal density gradient which drives a boundary flow, even at a vertical wall. The turbulent Phillips–Wunsch flow, in which there is a vigorous recirculation in the boundary layer, develops if the wall is sloping. This recirculation produces an additional dispersive mass flux along the wall, which also generates a net volume flux along the wall if the density gradient is non-uniform.

We investigate the effect of these boundary flows upon the mixing of the fluid in the interior of a closed vessel. The mixing in the interior fluid resulting from the laminar Phillips–Wunsch-driven boundary flow is governed by

$$\rho_t = \frac{\kappa_m}{A}(\rho z A)_z.$$

The turbulence-driven boundary flow mixes the interior fluid according to

$$\rho_t = \frac{1}{A}\left(\kappa_e \rho z \int \delta \, \mathrm{d}s\right)_z.$$

Here ρ is the density, κ_m and κ_e are the far-field (molecular) and effective boundary (eddy) diffusivities, including the dispersion, A is the cross-sectional area of the basin and $\int \delta \, \mathrm{d}s$ is the cross-sectional area of the boundary layer. The interior fluid is only mixed significantly faster than the rate of molecular diffusion if there is a turbulent boundary layer at the sidewalls of the containing vessel which either (i) varies in intensity with depth in the vessel or (ii) is mixing a non-uniform density gradient. These mixing phenomena are consistent with published experimental data and we consider the effect of such mixing in the ocean.

1. Introduction

Recently, there has been much interest in the problem of boundary-driven mixing to investigate whether flows generated at fluid boundaries can enhance the mixing of an otherwise quiescent fluid. Such boundary-driven mixing was first suggested by

† Present address: The Institute of Theoretical Geophysics, Department of Applied Mathematics and Theoretical Physics, University of Cambridge, Silver Street, Cambridge CB3 9EW, UK.

Munk (1966) as a potentially important mechanism in the complex process of deep ocean mixing. Since then, there have been several studies describing particular boundary mixing processes, and we briefly outline the history of these investigations below. In 1970, Phillips and Wunsch independently realized that a boundary current occurs in a stratified fluid at a sloping, insulating wall; this is because the isopycnals must be perpendicular to the wall and therefore horizontal density gradients arise near the wall. We will refer to this type of flow as the Phillips–Wunsch flow; it is a molecular process. Thorpe (1987) extended this solution to apply to a rotating fluid, and showed that in addition to the boundary current, an interior geostrophic flow, uniquely determined by the Phillips–Wunsch flow, is established parallel to the wall.

Armi (1978) rekindled interest in the subject of boundary mixing with some observations of mixing, caused by topography on the Sohm abyssal plain, north-east of Bermuda. In these observations, the vertical density profile had a step-like structure, which was interpreted as a record of the increased mixing of the fluid at some earlier time when it passed by topography. This work motivated several investigations into the effects of boundary-driving mixing; however, in most of the subsequent theoretical and experimental studies of mixing the fluid is assumed to have no large-scale organized motion away from the boundaries; the only large-scale, organized motions present are those induced by the boundary. This simplification allows the effect of the boundary-generated flows upon the mixing of the ocean interior to be studied in isolation and their importance estimated. Boundary-generated flows may be important in the mixing of a number of deep ocean basins, for example the Santa Monica Basin (Ledwell, Watson & Broecker 1986) in which the effects of meso-scale eddies and other currents are not as strong as in the open ocean. Ultimately, such models of the mixing caused by boundary-generated flows will be synthesized with models of mixing in currents passing beside the boundaries. Boundary-generated flows may be induced either (i) by the Phillips–Wunsch mechanism which occurs essentially because the boundary is sloping as explained above (Phillips 1970; Wunsch 1970), or (ii) because there is a turbulent boundary layer at the boundary, which mixes the fluid near the boundary more rapidly than in the interior. In a non-uniform density gradient, this process results in a larger rate of accumulation or diminution of the diffusing component near the wall as compared to the interior of the fluid. This produces horizontal density gradients which drive a boundary flow (Wunsch 1970; Ivey & Corcos 1982; Phillips, Shyu & Salmun 1986). Such turbulent boundary layers might be produced, for example, by internal waves interacting with the boundary (Eriksen 1985; Garrett & Gilbert 1988). Several analogue laboratory experiments, which have been undertaken to investigate boundary-driven mixing, have used oscillating grids to produce turbulent boundary layers near the sidewalls (Ivey & Corcos 1982; Thorpe 1982; Ivey 1987*a*; Phillips *et al.* 1986; Salmun & Phillips 1990).

Ivey & Corcos (1982) and Thorpe (1982) both carried out experiments in which they investigated the mixing caused by the presence of a grid-generated turbulent boundary layer adjacent to a vertical wall in a stratified fluid. They both showed empirically that the net vertical mass flux of the diffusing component scales as the boundary-layer eddy diffusivity rather than the much smaller interior molecular diffusivity. Phillips *et al.* (1986) extended this work by investigating experimentally the mixing produced by a grid-generated turbulent boundary layer along a sloping wall; Salmun & Phillips (1990) recently continued this study by investigating the effect of varying the slope of the boundary. Ivey (1987*a*) conducted experiments in which a cylindrical body of fluid, with a turbulent, sidewall boundary layer, was

rotated. These later studies confirmed that the net vertical mass flux of the diffusing component scales as the boundary eddy diffusivity.

Phillips *et al.* (1986) also presented a theoretical analysis of the turbulent boundary layer. They noticed that with large eddy diffusion coefficients near the boundary, the Phillips–Wunsch (1970) boundary flow becomes more intense, with a strong internal counter-flowing circulation developing near the boundary. Such an internal circulation leads to an alongslope turbulent dispersive mass flux, through a similar process to that described by Taylor (1954). Garrett (1990) investigated the turbulent boundary layer theory of Phillips *et al.* (1986) in more detail. He focused upon the case of *a uniform density gradient* and studied both the alongslope turbulent diffusive mass flux and the alongslope dispersive mass flux, which arise on a gently sloping boundary in the turbulent boundary layer. He showed that the total vertical mass flux equals the alongslope turbulent diffusive and dispersive mass fluxes; the alongslope dispersive flux is smaller than the cross-slope turbulent diffusive flux and so the net effect of the circulation is to lower the total vertical mass flux below that which would be produced by the purely turbulent diffusion acting on horizontal isopycnals. However, even though there is a turbulent mass flux along the boundary, Phillips *et al.* (1986) showed that in a uniformly stratified fluid, there is no increase in the volume flux along the boundary above that due to the molecular Phillips–Wunsch flow; therefore, it does not induce a return flow in the interior fluid.

Following Wunsch (1970) and Ivey & Corcos (1982), Phillips *et al.* also noted that in a non-uniform, vertical density gradient the boundary-driven mixing does generate a net volume flux along a sloping boundary, in addition to the Phillips–Wunsch flow. This second boundary flow mechanism is produced by the mechanism (ii) described above when the alongslope turbulent diffusive and dispersive mass fluxes diverge; it is a similar mechanism to that observed at a vertical wall in the experiments of Ivey & Corcos (1982) and Thorpe (1982). We develop the work of Garrett (1990) and show that in fact both the alongslope turbulent diffusive mass flux and the alongslope dispersive mass flux may be important, with the diffusive flux dominant at large slope angles.

Most of the work cited above focused upon the details of the mixing in the boundary layer, and the boundary-layer flows associated with such mixing. Several authors have deduced values for the interior diffusity, $\kappa_{\rm int}$ based on these boundary-flow analyses, following Armi (1978), who suggested that $\kappa_{\rm int} = \kappa_{\rm b} A_{\rm b}/A_{\rm int}$, where $A_{\rm b}/A_{\rm int}$ is the ratio of the area of the boundary layer to the whole basin and $\kappa_{\rm b}$ is the boundary-layer eddy diffusivity. Given the importance of boundary mixing, it seems timely to analyse in detail the manner in which such boundary currents affect the mixing of the fluid in the interior of a basin, away from the boundary. This is the main object of this paper. If there is a net volume flux up the slope associated with the boundary mixing, then in a closed basin there will be an equal but opposite return flow in the interior of the basin. We use the expressions for the interior return flow to derive advection–diffusion equations for the mixing in the interior fluid when there is both laminar and turbulent boundary-layer flow. The two regimes of boundary-driven mixing are shown to predict vastly different mixing rates in the interior. In this way, we are able to predict the manner in which the interior density profile evolves; the solutions we obtain are consistent with the published experimental data on boundary mixing.

We have arranged the present paper as follows. In §2 we review the laminar Phillips–Wunsch flow, deduce the bulk return flow in the interior of the fluid and derive the advection–diffusion equation describing the *mixing of the interior fluid*. We

present some simple examples which identify the key novel features of such mixing of the interior. In §3, we deduce that even with a turbulent boundary layer, the Phillips–Wunsch mechanism acting on a uniform density gradient cannot increase the rate of mixing of the interior beyond that timescale determined by the interior diffusivity; this is consistent with Thorpe (1987). We then contrast this with the situation in which the density gradient is nonlinear and there is a turbulent boundary layer. We present a local analysis for the turbulence-generated boundary flow at a vertical wall, in §4, following the approach of Phillips *et al.* (1986). Next, we derive and analyse the advection–diffusion equation describing the interior mixing produced by this turbulence-generated boundary flow. We show that this theory is consistent with the experiments of Ivey & Corcos (1982) and Thorpe (1982) and present some similarity solutions which elucidate the peculiar features of such mixing. Following Garrett (1990), we investigate both the diffusive and dispersive mass flux which develops in a sloping, turbulent boundary layer as a result of the recirculating boundary flow which develops. We show that when these mass fluxes diverge, the slope of the boundary determines whether the diffusive or dispersive mass flux dominates the net boundary-layer flow, and therefore the interior mixing. We conclude by investigating how such boundary-driven flows may affect the mixing of a constant source of fluid input at the bottom of a basin and discuss the relevance of these mixing phenomena in the oceanic context. In an Appendix, we present a simple bulk model of the turbulence-driven boundary flow along a vertical wall and suggest that in a rotating system a turbulence-driven geostrophic zonal flow may develop in a similar fashion to that produced by the Phillips–Wunsch flow (Thorpe 1987).

2. Interior mixing driven by the Phillips–Wunsch flow

In the present study we consider a non-rotating fluid in which one diffusing component determines the density; all the processes we describe are related to single-component convection. The analogous problem in double-diffusive convection results in a quite different flow field (Turner 1979; Kerr 1989), but we do not discuss this here.

Phillips (1970) and Wunsch (1970) studied the boundary-layer flow which develops along a sloping sidewall in a stratified fluid. The flow develops because of the boundary condition of zero normal mass flux at the wall; this causes the isopycnals near the wall to deflect away from the horizontal thereby producing a horizontal density gradient and a flow.

They showed that the volume flux through the boundary layer associated with this flow satisfies

$$\int_0^\infty v \, \mathrm{d}x = \kappa \cot\theta, \tag{2.1}$$

where the geometry of the system is shown in figure 1. This volume flux is purely a function of the slope of the wall and the molecular diffusivity, κ, but requires that the interior density gradient, $\partial\rho_0/\partial z$, be non-zero and approximately constant over a vertical scale of the same order as the boundary-layer width, $\delta \sim (N^2 \sin^2\theta/\kappa\mu)^{-\frac{1}{4}}$. If the Prandtl number, ν/κ, is large the boundary flow is stable. However, as mentioned by Phillips (1970), if the Prandtl number is very small, for example in a metallic system, then this boundary flow may become unstable. As $\theta \to 0$, the boundary layer becomes very wide and the theory breaks down.

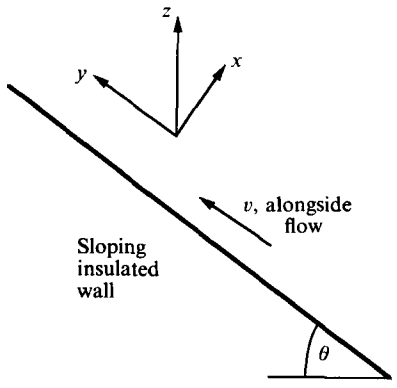

FIGURE 1. Diagram defining the coordinate system for the analysis of the boundary flows.

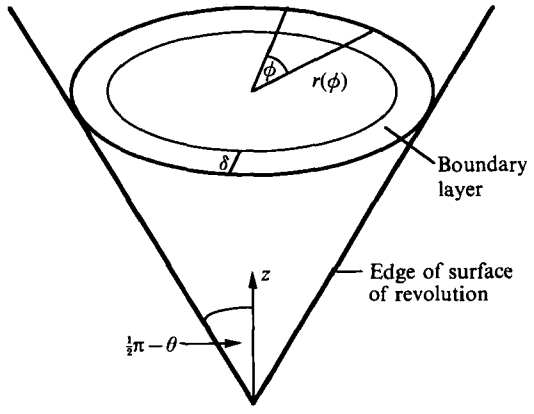

FIGURE 2. Diagram showing the boundary-layer structure at the outer edge of a surface of revolution containing the fluid.

Given the boundary volume flux, (2.1) we calculate a new advection-diffusion equation governing the transport processes in the interior. Consider a vessel with sloping walls in which the radius of curvature of the vessel is everywhere much larger than the boundary-layer width. From (2.1) it follows that the total volume flux through the boundary layer is

$$\text{Flux} = \int_0^{2\pi} \kappa \cot(\theta(\phi))\, r(\phi)\, \mathrm{d}\phi, \tag{2.2}$$

where ϕ is the angle of the radius vector shown in figure 2. By mass conservation, the interior return flow in a closed basin is

$$W = -\frac{\kappa \mathrm{A}_z}{\mathrm{A}} \tag{2.3}$$

where A_z is the cross-sectional area of the basin, $A_z = \frac{1}{2}\int_0^{2\pi} r^2(\phi,\ z)\, \mathrm{d}\phi$. For example, in a symmetrical surface of revolution, $\cot(\theta(\phi)) = \cot(\theta)$, $r(\phi, z) = r(z)$ and the net flux in the boundary layer is

$$F = 2\pi\kappa r \cot\theta \tag{2.4}$$

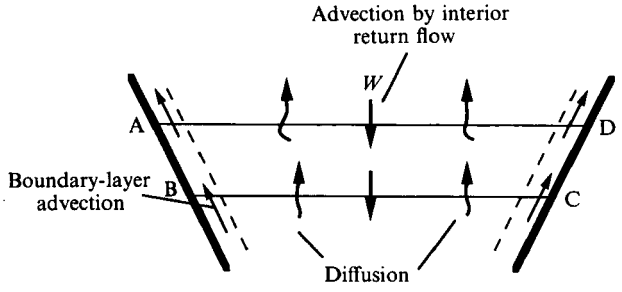

FIGURE 3. Diagram showing the three contributions to the mass balance in a fixed control volume in the fluid. These are the vertical diffusive flux (wiggly arrows), the vertical advected flux (vertical arrows) and the flux input due to the flow in the sidewall (sloping arrows).

Hence the bulk return flow in the interior is

$$W = -2\kappa \frac{r_z}{r}. \tag{2.5}$$

From (2.3), the local advection-diffusion balance in the interior gives the interior mixing equation

$$\rho_t - \kappa \rho_z \frac{A_z}{A} = \kappa \rho_{zz}. \tag{2.6}$$

There is an alternative derivation of the interior mixing equation which is quite instructive. For this, we require a second result of Phillips (1970), who showed that the advected mass flux due to the boundary-layer flow satisfies

$$\frac{\partial}{\partial y}\left(\int_0^\infty \rho v \, \mathrm{d}x\right) = \kappa \frac{\partial \rho_0}{\partial z} \cos(\theta). \tag{2.7}$$

This result may be simply stated that the gradient of the mass flux supplied by the boundary layer exactly balances the diffusive flux required by the interior. Therefore as a parcel of fluid is carried up the slope, its density decreases so that its density difference with the interior remains a function only of the local boundary slope and the local ambient density gradient.

The equation for the conservation of mass across a thin, horizontal control volume, ABCD, as shown in figure 3, is

$$\frac{\partial(\rho A)}{\partial t} = \kappa \frac{\partial}{\partial z}\left(A \frac{\partial \rho}{\partial z}\right) - \frac{\partial}{\partial z}(W \rho A) - \kappa \frac{\partial}{\partial z}\left(\rho \frac{\partial A}{\partial z}\right). \tag{2.8}$$

The first term on the right-hand side is the change in the interior diffusive flux with height, the second term is the change in the advective flux with height in the interior and the third term is the change in the advected mass flux in the boundary layer per unit height, equation (2.7). It follows from (2.3) that the change in the advective flux in the interior is equal and opposite to the change in the advective flux in the boundary layer (assuming that A_z/A_{zz}, $\rho_z/\rho_{zz} \gg \delta$, in order to use the Phillips–Wunsch-type solution). Therefore the last two terms cancel and the equation for the mass transfer in the interior is

$$\frac{\partial \rho}{\partial t} = \frac{\kappa}{A} \frac{\partial}{\partial z}\left(A \frac{\partial \rho}{\partial z}\right). \tag{2.9}$$

This is identical to the local advection–diffusion equation for the interior, (2.6). The mechanism of mass transfer involves both a diffusive and an advective ingredient. Because of the exact balance between the bulk advective mass transport in the interior and the advected mass flux in the boundary layer the net mass transport across any horizontal surface is purely by diffusion. The mean return flow in the interior is necessary in order that the interior isopycnals remain horizontal.

The effect of the advection in the interior may be readily understood by considering the case in which $A_z > 0$. In this case, in steady state, with a given flux applied to the bottom surface and removed from the top surface of the vessel, $A\rho_z = constant$. Thus the isopyncals move further apart as z, and hence the tank radius, increases. This stretching of the isopycnals can only be effected by the bulk advective flow $-\kappa A_z/A$, which acts downwards. By advecting less of the relatively light fluid downwards per unit width, as z increases, the isopyncals are less compressed as z increases; therefore the diffusive mass flux per unit width decreases as z increases.

If part of the bounding wall becomes vertical then there will be no boundary flow adjacent to this part of the wall. At such a portion of the boundary, the interior return flow decelerates to zero owing to the no-slip boundary condition and the boundary-flow has the form

$$v(x) = v(\infty)\,[1+\exp(-x/\delta)\,(\sin(x/\delta)-\cos(x/\delta))], \tag{2.10}$$

and

$$\rho(x) = \frac{2\nu\rho_0}{g}\delta^{-2}v(\infty)\exp(-x/\delta)\,[\cos(x/\delta)+\sin(x/\delta)], \tag{2.11}$$

where $\delta = (1/\sqrt{2})\,(N^2/\kappa\mu)^{-\frac{1}{4}}$ and $v(\infty)$ is the interior flow. We have mentioned this effect for completeness; it has a negligible effect on the mixing.

We now investigate the steady-state, interior density profiles in a number of simple vessel geometries. We express the solutions in terms of $\rho(0)$ and $\rho_z(0)$ where $z = 0$ represents the base of the vessel. If $A_{zz} \neq 0$ or $\rho_{zz} \neq 0$, then the volume flux transported in the turbulent boundary layer may change with depth; however, as long as the lengthscales, $\delta_A \sim A_z/A_{zz}$ and $L \sim \rho_z/\rho_{zz}$, over which A_z and ρ_z change are large compared to the boundary-layer width, δ, this does not affect the local boundary-layer analysis and the slow interior variations are accommodated in the theory implicitly.

(i) When the vessel has the form of a long channel, whose sidewalls are in the shape of a wedge with linear slope, $L = L_0 + \alpha z$, the interior advection–diffusion equation is simply

$$\rho_t = \frac{\kappa}{L}(\rho_z L)_z, \tag{2.12}$$

and the steady solution is

$$\rho(z) = \frac{L_0\rho_z(0)}{\alpha}\ln\left(\frac{(L_0+\alpha z)}{L_0}\right)+\rho(0). \tag{2.13}$$

This result may be used in an interesting problem which elucidates the importance of the Phillips–Wunsch boundary flow in determining the interior density distribution. Consider a plate suspended, with an inclination to the vertical, in a tank with vertical sidewalls, such that the plate does not touch the upper or lower surface of the fluid. In this case, a Phillips–Wunsch flow develops on both sides of the plate (figure 4*a*). Since the plate neither reaches the upper nor lower boundary of the

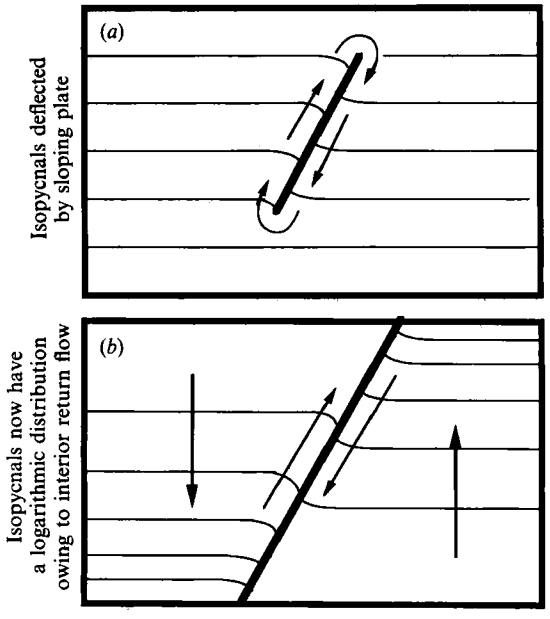

FIGURE 4. (*a*) Schematic of the boundary flow and the isopyncals when an inclined plate lies entirely within the upper and lower surfaces of a vessel containing stratified fluid. (*b*) Corresponding sketch when the sloping plate does intersect the upper and lower boundaries. Now, as a result of the counterflowing boundary flows, the isopyncals become logarithmically spaced, with the stratification of the overlying fluid increasing towards the base and the stratification of the underlying fluid increasing towards the top. Note the figure shows the stratification only schematically.

container, this boundary flow does not force a return flow in the interior fluid; instead the upflow on one side of the plate flows into the downflow on the other side of the plate. This generates a net circulation around the plate, but no flow in the interior fluid. The isopycnals in the interior are equispaced, as they would be in the purely diffusive solution (figure 4*a*). This solution is possible since the mass flux provided by the boundary-layer flow to the interior fluid, per unit height, (2.7), equals that change in the total interior diffusive flux due to the changing cross-sectional area of the interior.

This situation may then be contrasted with the analogous problem in which the inclined plate actually meets the upper and lower boundaries of the fluid. Now, the boundary-layer flows on either side of the plate are not connected; instead they drive a mean return flow in the interior (figure 4*b*), and the logarithmic density profile (2.13), increasing in a different direction on each side of the plate is established. The qualitative form of the solution is sketched in figure 4(*b*).

An interesting application of this result, suggested by O. M. Phillips (private communication, 1990), is to a loosely packed gravel bed (in this context, loosely packed means that the interparticle spacing exceeds the boundary-layer width δ and all the fluid is in communication at all heights). If the net liquid fraction in the gravel bed changes with height, then the overall density profile, will, in general, be nonlinear. If the liquid fraction at depth z is $\phi(z)$ then the density profile is determined by

$$\rho_t = \frac{1}{A\phi}(A\phi\rho z)_z \tag{2.14}$$

in a vessel of cross-sectional area $A(z)$. This is identical to (2.6) with the area of fluid at each height now determined by both the liquid fraction and the cross-sectional area of the vessel.

Other very simple geometries have steady-state density profiles which are far from linear.

(ii) If the channel has the shape of a semicircle $L = (a^2 - z^2)^{\frac{1}{2}}$ then the steady-state density profile becomes

$$\rho(z) = \rho(0) + a\rho_z(0)\sin^{-1}(z/a). \tag{2.15}$$

(iii) If the vessel is a symmetric surface of revolution with radius $r = \alpha(z/z_0)^n$ then the density distribution has the form

$$\rho(z) = \rho(0) + \rho_z(0)\left(\frac{z}{z_0}\right)^{1-2n}\left(\frac{z_0}{1-2n}\right). \tag{2.16}$$

3. Timescale of mixing by the Phillips-Wunsch flow

There has been much discussion in the literature as to the effectiveness of such boundary flows in mixing the interior fluid (Wunsch 1970; Garrett 1990). In the simple situation we discussed in §2, in which the diffusion coefficients are constant, the interior advection–diffusion equation (2.6) shows that the timescale for the mixing is given by the interior molecular diffusivity κ together with the typical radius and depth of the basin, R and H say. Therefore a stratified fluid will mix in a time τ of the order of

$$\tau \sim \min\left(\frac{HR}{\kappa}, \frac{H^2}{\kappa}\right). \tag{3.1}$$

Even though the density profiles become very nonlinear, the Phillips-Wunsch boundary flow cannot enhance the rate of mixing of the interior fluid beyond the diffusive timescale. Note however, that in a vessel with sloping sidewalls, in which $H \gg R$, the Phillips–Wunsch flow reduces the mixing timescale from H^2/κ, which is appropriate for a vertically walled tube, to HR/κ; a reduction proportional to the aspect ratio of the tube (Phillips 1970); this result has some similarity with the Boycott effect in which particles may be rapidly sedimented out of suspension in a liquid in a tube by tilting the tube (Nir & Acrivos 1990) since both processes are the result of zero mass flux through the wall.

The bulk interior motion does not change the rate of mixing compared to the purely diffusive timescale even if there is significant bottom topography. This is because the process remains essentially diffusive. For example, consider the situation in which the floor of the vessel (e.g. the ocean basin) has a series of obstructions (e.g. sea-mountains). If the vessel has cross-sectional area A and there are n vertical, conical obstructions of semi-angle α and bottom radius b placed on the floor then the interior mixing equation is

$$\frac{\partial \rho}{\partial t} = \left(\frac{\kappa}{A - n\pi[b - z\tan\alpha]^2}\right)\frac{\partial}{\partial z}((A - n\pi[b - z\tan\alpha]^2)\rho_z). \tag{3.2}$$

Therefore, although the steady density profile is nonlinear, the effective diffusion coefficient for the mixing scales as κ as in the case with a flat bottom.

The situation becomes more complex if there is a turbulent boundary layer near the sloping walls. As briefly described in the introduction, when there is a turbulent boundary layer in which the eddy diffusion coefficients decay with distance from the

wall, the Phillips–Wunsch flow develops a counterflowing circulation (Phillips *et al.* 1986). This produces a dispersive mass flux in addition to the turbulent diffusive mass flux. If the interior density gradient is non-uniform the rate of accumulation/diminution of the diffusing component near the wall will be greater than that in the interior fluid owing to the greater mass flux near the wall; even at a vertical wall (in which case there is negligible dispersive mass flux) this generates a horizontal density gradient which produces a net boundary current (Wunsch 1970; Ivey & Corcos 1982). We consider this turbulence-induced flow in the remaining sections of the paper.

However, before launching into this discussion, we note that when the interior density gradient is constant, even the turbulent Phillips–Wunsch flow does not cause the interior to mix more rapidly than the timescale determined by the molecular diffusion. Phillips *et al.* (1986) and Thorpe (1987) showed that when $\rho_{zz} = 0$, even with a turbulent boundary layer, the net volume flux through the boundary scales as

$$\int_0^\infty v \, \mathrm{d}x = \kappa_e(\infty) \cot(\theta). \tag{3.3}$$

This is purely a function of the far-field diffusivity, $\kappa_e(\infty)$ (which equals the molecular diffusivity κ_m in a quiescent fluid) and the slope of the wall. Even though there is a turbulent diffusive and dispersive mass flux, the turbulent recirculating flow in the boundary produces no net volume flux.

In this case, with $\rho_{zz} = 0$, the equation for the mixing in the interior reduces to

$$\rho_t = \kappa_m \frac{A_z}{A} \rho_z. \tag{3.4}$$

The only solution of this equation which maintains a constant density gradient arises when $A = A_0 \exp(z + \alpha z^2)$ and is $\rho(z, t) = \rho(0, 0) \exp[2\kappa_m \alpha t](1 + 2\alpha z)$. In this rather contrived example, we see that the boundary flow does not increase the rate of interior mixing beyond that determined by the interior diffusivity, since the advective flow scales as the interior diffusivity, and not the larger, boundary eddy diffusivity. For any other shape of the containing vessel, the density gradient rapidly becomes non-uniform, and the mixing process becomes dominated by the turbulence-generated boundary flows.

4. Turbulent mixing at a vertical wall

Consider the situation in which there is a *vertical* wall bounding a nonlinearly stratified fluid, with a turbulent boundary layer adjacent to the wall. In this case no Phillips–Wunsch flow may develop. We assume that the mean flows are weak so that we may linearize the momentum equation and we parameterize the turbulent fluctuations with an eddy diffusivity and viscosity (Phillips *et al.* 1986). Using the coordinate system defined in figure 1 with $\theta = \frac{1}{2}\pi$ so that $z = y$, the mass conservation equation is

$$u \frac{\partial \rho}{\partial x} + v \frac{\partial \rho}{\partial y} = \nabla \cdot (\kappa_e \nabla \rho), \tag{4.1}$$

while the linearized vorticity equation is

$$g \left(\frac{\partial \rho}{\partial x} \right) = \rho(0) \left(\frac{\partial}{\partial x} - \frac{\partial}{\partial y} \right) \nabla \cdot (\nu_e \nabla v) \tag{4.2}$$

For clarity, we write $\rho(x, y) = \rho_0(y) + \rho_1(x, y)$. As in §2, we consider the situation in which the boundary-layer width, δ, is much less than the vertical scale, L, over which the ambient density gradient changes, $L \sim \rho_{0z}/\rho_{0zz}$, and we deduce that $\partial/\partial y \ll \partial/\partial x$ and $u \ll v$. The term $(\boldsymbol{u}\cdot\boldsymbol{\nabla})\rho_1$ in (4.1) is small if $\rho_{0yy}^2(\kappa_e \nu_e \rho_0)^{\frac{1}{2}} \ll \rho_y^{\frac{5}{2}} g^{\frac{1}{2}}$ (in §5 we derive a scaling for δ which shows that this is equivalent to $\delta \ll L$). In this case, to leading order, (4.1) and (4.2) become

$$v\frac{\partial \rho_0}{\partial y} = \frac{\partial}{\partial y}\left(\kappa_e \frac{\partial \rho_0}{\partial y}\right) + \frac{\partial}{\partial x}\left(\kappa_e \frac{\partial \rho_1}{\partial x}\right) \tag{4.3}$$

and

$$g\frac{\partial \rho_1}{\partial x} = \rho(0)\frac{\partial^2}{\partial x^2}\left(\nu_e \frac{\partial v}{\partial x}\right), \tag{4.4}$$

where $v = \psi_x$ and $u = -\psi_y$. From (4.3) and (4.4) we can determine the boundary-layer velocity, the density field and the boundary-layer thickness; the boundary-layer properties scale as

$$v \sim \frac{\kappa_e}{L}; \quad \delta \sim \left(\frac{\rho(0)\,\nu_e \kappa_e}{g\rho_{0y}}\right)^{\frac{1}{4}}, \quad \rho_1 \sim \frac{\rho(0)\,\nu_e \kappa_e}{g\delta^2}\frac{\rho_{0yy}}{\rho_{0y}}, \tag{4.5}$$

where $\rho(0)$ is a typical value of the density. At $x = 0$, $\partial\rho/\partial x = 0$ and $v = u = 0$, while for $x > \delta$, $\rho_1, u, v \sim 0$. If we integrate (4.3) from $x = 0$ to a point beyond $x = \delta$, where δ is the boundary-layer width defined such that $\kappa_e(x) \sim 0$ for $x > \delta$, we obtain

$$\psi(\delta)\frac{\partial \rho_0}{\partial y} \sim \frac{\partial}{\partial y}\left(\int_0^\delta \kappa_e(x)\,dx \frac{\partial \rho_0}{\partial y}\right). \tag{4.6}$$

$\psi(\delta)$ is the leading-order asymptotic approximation for $\psi(\infty)$, the volume flux per unit cross-slope length of the boundary layer, assuming that $\delta\overline{\kappa}_e \gg R\kappa_m$, where R is the width of the vessel and κ_m the interior, molecular diffusivity and $\delta\overline{\kappa}_e = \int dx \kappa_e(x)$. Integrating to a point just beyond $x = \delta$ ensures that the integral is convergent (cf Garrett 1990).

We deduce that the total volume transport in the turbulent boundary layer, integrated around the sidewalls of a closed basin, is

$$\int ds\,\delta\psi(\infty) \sim \frac{\int ds\,(\delta\overline{\kappa_e}\rho_{0y})_y}{\rho_{0y}}, \tag{4.7}$$

where $\int \delta\,ds$ is the area of the boundary layer integrated around the surface of the vessel at height z. We have assumed that $\delta(\phi) \ll r(\phi)$ so that our local two-dimensional analysis holds. McDougall (1989) obtained a simplified form of (4.7) for the boundary-layer volume flux using a bulk model to describe the boundary layer, in a similar fashion to the first part of the Appendix.

This turbulence-induced boundary flow forces a mean return flow in the fluid interior given, as in §2, by the expression

$$W = \frac{\int ds\,(\delta\overline{\kappa_e}\rho_{0y})_y}{\rho_{0y}\int dA}, \tag{4.8}$$

where ds is an element of the surface at depth y and $\int dA$ is the cross-sectional area of the basin at depth y. W is non-zero only if either the interior density gradient is

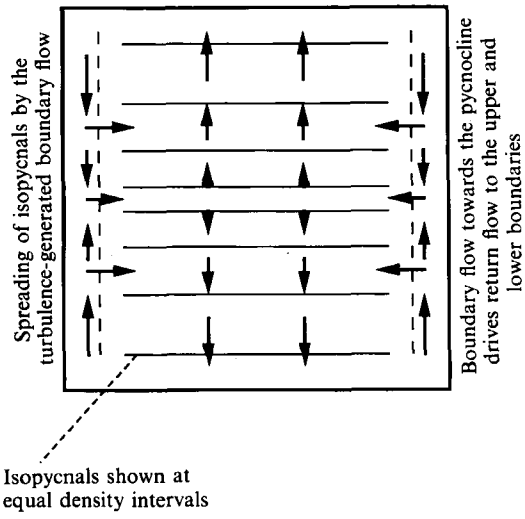

FIGURE 5. Schematic diagram showing illustrating the mixing of the interior fluid by the boundary-driven flow. In the diagram shown the initial density profile was a symmetrical pycnocline.

non-uniform or the intensity of the turbulent mixing, $\delta\overline{\kappa}_e$, varies with height. If W is non-uniform then the interior fluid may be mixed advectively. The advection–diffusion equation for the interior has the form

$$\rho_t - \frac{\int \mathrm{d}s(\delta\overline{\kappa}_e\rho_y)_y}{\int \mathrm{d}A} = \kappa_m\rho_{yy}. \tag{4.9}$$

This is quite different from the equation (2.6) derived in §2 for the laminar Phillips–Wunsch flow; in the present case, the effect of the advective flux may far exceed the effect of the interior (molecular) diffusion if

$$\int \mathrm{d}s \int_0^\delta \mathrm{d}x\kappa_e(x) \gg \int \mathrm{d}A\kappa_m. \tag{4.10}$$

In a cylinder of radius R ($\gg \delta$) with vertical walls, (4.9) reduces to

$$\rho_t = \kappa_m\rho_{yy} + 2\frac{(\delta\overline{\kappa}_e\rho_y)_y}{R}. \tag{4.11}$$

The boundary flow may either entrain or detrain into the interior of the fluid body. The detrainment velocity is

$$\frac{\mathrm{d}}{\mathrm{d}y}\psi(\delta) \sim \frac{\mathrm{d}}{\mathrm{d}y}\left(\frac{(\delta\overline{\kappa}_e\rho_y)_y}{\rho_y}\right). \tag{4.12}$$

Note that (4.9) accounts for this detrainment implicitly. The buoyancy jump across the boundary layer is given from (4.4) by

$$\rho_1(0) \sim \frac{\rho(0)}{g}\frac{\partial}{\partial x}\left(\nu_e\frac{\partial v}{\partial x}\right)\Big|_0 \tag{4.13}$$

since $\rho_1(\delta) \sim 0$.

One very interesting feature of the mixing, described by (4.9), is that in the limit (4.10) the process is not diffusive. The mixing of the interior fluid is effected by vertical variations in the mean return flow in the interior; such variations arise as a result of entrainment or detrainment from the boundary-layer flow if the cross-sectional area of the basin is constant. If the return flow in the interior changes with depth, the isopyncals are advected vertically at different rates such that they are spread further apart or compressed and so the interior density gradient changes, as originally discussed by Wunsch (1970). This process is shown schematically for a pycnocline in figure 5; it is consistent with the observations and discussion of Ivey & Corcos (1982) and Ivey & Nokes (1989). Following Ivey & Corcos (1982), in our model we assume that the lateral intrusions, which result from the variations of the mean vertical volume flux with height in the boundary layer, spread uniformly across the vessel and we can thereby predict the interior flow field.

In the Appendix we present a simple, horizontally averaged bulk model describing the turbulence-generated boundary flow, similar in approach to McDougall (1989). This is instructive because it predicts the same results as the more detailed model of this section but only uses the global conservation of mass.

5. Comparison of the interior mixing model with experiment

In this section we compare the theoretical model introduced in §4 with some laboratory experiments reported by Ivey & Corcos (1982) and Thorpe (1982). In these experiments a grid was oscillated at a vertical sidewall of a tank containing a stratified fluid. The initial stratification consisted of either a linear density gradient or a pycnocline. Thorpe (1982) parameterized the eddy diffusivity and boundary layer width using the experimental results of Hopfinger & Toly (1976), who investigated grid turbulence in a homogeneous fluid. He argued that the boundary-layer width is determined by the point at which the timescale of an eddy exceeds that due to the stratification; at this point the turbulent eddies collapse under the stratification. Assuming that the motion within the boundary layer is independent of the stratification, Hopfinger & Toly's velocity and integral lengthscales may be used to give the scale for the boundary-layer thickness

$$\delta \sim a^{\frac{3}{4}} d^{\frac{1}{4}} \left(\frac{\omega^2 \rho_0}{-g\rho_y} \right)^{\frac{1}{4}}, \tag{5.1}$$

where a is the amplitude of oscillation, ω the frequency of oscillation and d the grid spacing. This is consistent with the model equation (4.5). It also follows from the work of Hopfinger & Toly that the eddy diffusivity in the boundary layer scales as the product of the integral lengthscale and the boundary-layer velocity;

$$\overline{\kappa_e} \sim \omega a^{\frac{3}{2}} d^{\frac{1}{2}}. \tag{5.2}$$

Combining these two results it readily follows that

$$\frac{\int \mathrm{d}s \overline{\kappa_e} \delta}{\int \mathrm{d}A} \sim \frac{\rho_0^{\frac{1}{4}} a^{\frac{9}{4}} d^{\frac{3}{4}} \omega^{\frac{3}{2}} \int \mathrm{d}s}{(-g\rho_y)^{\frac{1}{4}} \int \mathrm{d}A}. \tag{5.3}$$

Ivey & Corcos (1982) derived analogous scalings for the boundary layer and later Ivey (1987*a*) applied the results of Itsweire, Helland & Van Atta (1986) to derive the

same result. Using (4.9) and (5.3) we deduce that the advection–diffusion equation modelling the mixing of the interior fluid in the experiments of Ivey & Corcos (1982) is

$$\rho_t = \left[\gamma \frac{\int \mathrm{d}s}{\int \mathrm{d}A(-\rho_y)^{\frac{1}{4}}} + \kappa_\mathrm{m} \right] \rho_{yy} \tag{5.4}$$

in the limit $\rho_{0yy}^2(\kappa_\mathrm{e}\nu_\mathrm{e}\rho_0)^{\frac{1}{2}} \ll g^{\frac{1}{2}}\rho_{0y}^{\frac{5}{2}}$ (i.e. $L \gg \delta$), where $\gamma = \gamma_0 a^{3\alpha} d^{(3(1-\alpha))} \omega^{\frac{3}{2}} (\rho_0/g)^{\frac{1}{4}}$, γ_0 is constant and $\alpha = \frac{3}{4}$.

As in §2, there is an alternative derivation of the interior advection–diffusion equation (5.4). Given the total vertical mass flux, F, into and out of a control volume in the form of a horizontal slice which spans the whole cross-section of the vessel, we may derive the interior advection-diffusion equation by considering

$$\frac{\partial}{\partial t}\int \mathrm{d}A\rho = \frac{\partial F}{\partial y}. \tag{5.5}$$

The value F may be determined either from experiment or from theory. In this way, the global mixing equation for the ambient density, ρ_0, may be derived solely from the experimentally measured mass flux.

The vertical mass flux, F, predicted by our model satisfies

$$F = \int \mathrm{d}s\delta\overline{\kappa_\mathrm{e}}\frac{\partial\rho_0}{\partial y} + \int \mathrm{d}A\kappa_\mathrm{m}\frac{\partial\rho_0}{\partial y} + \int \mathrm{d}s\int_0^\delta v\rho_1\,\mathrm{d}x \tag{5.6}$$

where the first two terms represent the diffusive mass transfer in the boundary layer and interior respectively and the last term is the net advective mass flux due to the density anomaly between the boundary layer and the interior fluid. In the experiments reported by Ivey & Corcos (1982) and Thorpe (1982), the ratio of area of the interior of the basin to the area of the boundary layer satisfied

$$1 \ll \frac{\int \mathrm{d}A}{\int \mathrm{d}s\delta} \ll \frac{\overline{\kappa}_\mathrm{e}}{\kappa_\mathrm{m}}. \tag{5.7}$$

Thus it follows that the molecular diffusion in the interior is negligible. Furthermore, from the scalings given in (4.5), it follows that $\rho_1 v \ll (\partial\rho_0/\partial y)\kappa_\mathrm{e}$, so that the dispersive contribution to the mass flux is negligible. Therefore (5.6) may be simplified to

$$F \sim \int \mathrm{d}s\,\delta\overline{\kappa_\mathrm{e}}\rho_y \sim -\frac{4}{3}\gamma(-\rho_y)^{\frac{3}{4}}\int \mathrm{d}s. \tag{5.8}$$

This equation implies that asymptotically the net vertical mass flux is transported principally by turbulent diffusion through the boundary layer (i.e. the first term on the right-hand side of (5.6) is dominant). The dependence of the net mass flux upon ρ_y as predicted by (5.8) is the same as that measured experimentally by Ivey & Corcos (1982), Thorpe (1982) and Ivey (1987*a*).† This supports the physical model of §4.

† We note that there is some disagreement about the constant α in the expression for γ, (5.1); however, Thorpe (1982) pointed out that $\alpha = \frac{3}{4}$ is consistent, within experimental error, with all the experimental results.

From (5.5) and (5.8) the interior mixing is given by

$$\rho_t = \gamma \frac{\rho_{yy} \int \mathrm{d}s}{\int \mathrm{d}A(-\rho_y)^{\frac{1}{4}}}. \tag{5.9}$$

This is identical to the mixing equation (5.4) which was derived from the boundary-layer dynamics by consideration of the net volume flux in the boundary layer and hence the interior; this agreement is strong evidence to support the model of the boundary layer and interior return flow. As explained in §4, the flow field in the interior spreads the isopycnals so that the interior density profile evolves at the rate determined by the mass flux in the boundary.

Equation (5.9) has a similarity solution, using the combination $\eta = yt^{-\frac{4}{7}}$, in which ρ satisfies the ordinary differential equation

$$\rho_\eta = -\left(\frac{1}{(-\rho_{0\eta})^{\frac{1}{4}}} + \frac{1}{14\lambda}(\eta^2 - \eta_0^2)\right)^{-4}, \tag{5.10}$$

where $\lambda = \gamma \int \mathrm{d}s / \int \mathrm{d}A$. In this similarity solution, a pycnocline is predicted to spread approximately as $y \sim t^{\frac{4}{7}}$ in a tank with vertical sidewalls. This is different from purely diffusive mixing, in which a pynocline spreads as $z \sim t^{\frac{1}{2}}$. Note that this theory strictly only applies when $\delta \ll L$; using the boundary-layer scalings for a pynocline this occurs after a time $t \sim (\kappa_\mathrm{m} A/\kappa_\mathrm{e})\,(g\rho_y/\rho\nu_\mathrm{e}\kappa_\mathrm{e})^{-\frac{9}{64}}$, which is very soon after the start of the experiment.

Equation (5.10) may be solved analytically for a region $\eta \in (0, \infty)$ in which $\rho(0) = 1$ and $\rho(\infty) = 0$, for example by using the substitution $\eta = 14^{\frac{1}{2}}\lambda^{\frac{1}{2}} \tan(\phi)/(-\rho_{0\eta})^{\frac{1}{8}}$; in figure 6(*a*), we have plotted ρ as a function of η. The similarity solution breaks down with no-flux boundary conditions imposed at $z = 0$ and $z = H$. In figure 6(*b*), we plot the numerical solution of the advection–diffusion equation (5.9) with an initial condition of a pynocline. This shows how the solution diverges from the similarity form, as a result of the boundary influence and may also be compared with figure 6 of Ivey & Corcos (1982).

Ivey & Corcos (1982) first described the interior flow (their figure 12) and noted that since the lateral flow extends across the vessel interior, the lateral flow at position x away from the boundary has the value $u = U(L-x)/L$, where U is the detrainment velocity from the boundary layer and L is the width of the vessel, in two-dimensions, or radius, in three dimensions. Using our boundary-layer analysis, we can explicitly compute the interior flow as a function of the boundary-layer motion.

When a linear density profile is present in the tank, the no-flux boundary condition at the upper and lower boundaries produces the nonlinearity in the density profile. This drives a boundary-layer flow which rapidly spreads to the centre of the tank; the boundary layer near the top of the vessel is enriched with heavy fluid by turbulent mixing and sinks, while the boundary layer near the base of the tank is enriched in lighter fluid and rises. By conservation of mass, lateral intrusions develop as the two boundary flows converge near the middle of the vessel. However, at the upper and lower corners of the tank, an extra complication arises owing to the different rate of mixing at the corners compared with at a planar boundary.

With a pycnocline, the turbulence beside the wall causes the boundary layer above the interface to become enriched in heavy fluid and it sinks, while the fluid below the

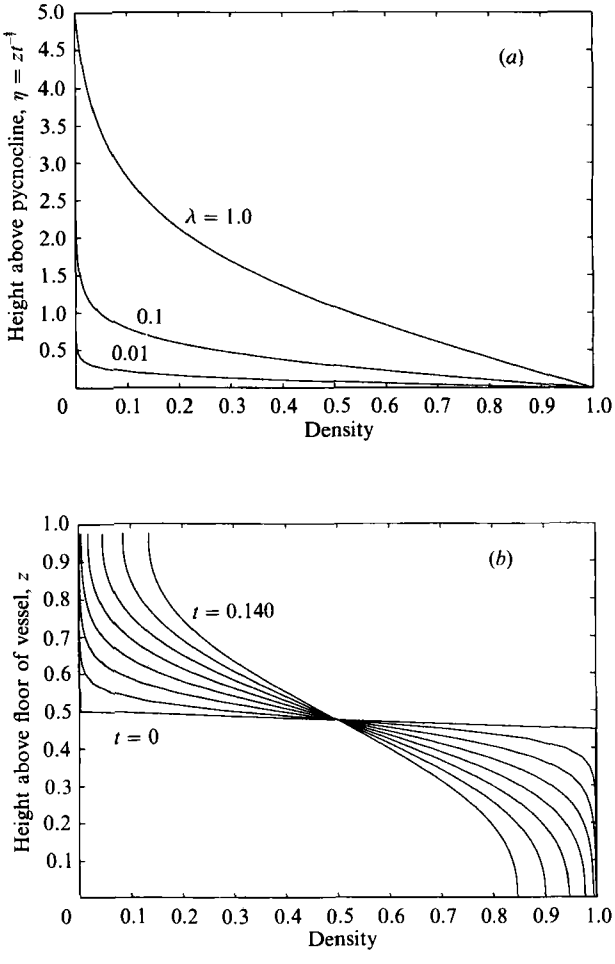

FIGURE 6 (a, b). For caption see facing page.

interface becomes enriched in light fluid and rises. These converging flows also drive lateral intrusions. In figure 6(c, d) (which is similar to figure 12 of Ivey & Corcos) we have plotted the stream function for the interior flow field for the mixing of a pynocline in both a two-dimensional geometry, as relevant for the Ivey & Corcos (1982) and Thorpe (1982) experiments, and also in a cylindrical vessel. In these plots we have used the similarity density profile of figure 6(a) with $\lambda = 1$.

We have calculated the rate of spread of the pynocline from the data reported by Ivey & Corcos (their figure 6) and this is shown in the present figure 7. Given the turbulent nature of the mixing, the data agree reasonably well with the solid line $z \sim t^{\frac{4}{7}}$ predicted by the above similarity theory, up to the time $\log(t) \sim 3$. However, beyond this point, the mixing is more rapid, possibly because the pycnocline has spread to the upper and lower horizontal boundaries and so the end effects enhance the rate of mixing. In addition, near the upper and lower corners the eddy diffusivities differ from those beside a planar wall (Ivey & Corcos 1982). This effect may also cause the experiment to evolve more rapidly than predicted by the similarity solution. The mass flux measurements are a more reliable test of the theory

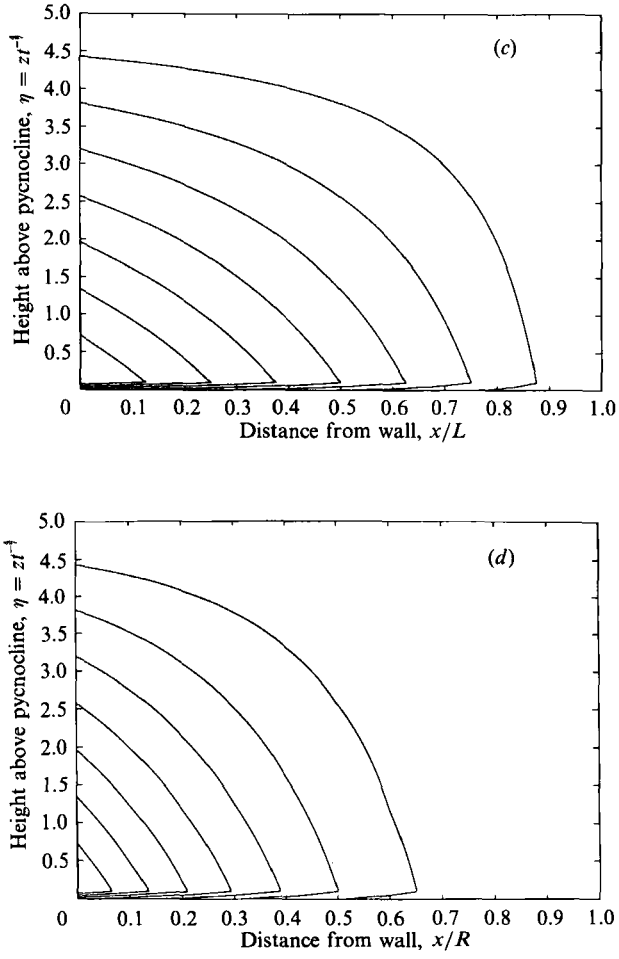

FIGURE 6. (*a*) The similarity solution (5.10) for the dimensionless density in the interior of the fluid produced by the mixing from the turbulence-driven boundary flow at a vertical wall. Solutions are given for $\lambda = 1.0$, 0.1 and 0.01. (*b*) The evolution of the density profile with time, as predicted by (5.9), incorporating the effects of the zero-flux boundary conditions. Profiles are given at the non-dimensional times 0, 0.005, 0.015, 0.030, 0.050, 0.075, 0.105 and 0.140 for $\lambda = 1$. Compare with figure 6 of Ivey & Corcos (1982). (*c*, *d*) Streamlines for the flow above a pynocline which is being mixed in (*c*) a two-dimensional channel of width L and (*d*) a cylindrical vessel of radius R.

because the mass flux is a vertically averaged measurement and errors are smoothed out in contrast to a local measurement of the rate of spread of an individual pynocline. We have shown in this section that the theory which predicts the interior volume flux and the interior mixing equation is consistent with the mass flux measurements of both Ivey & Corcos (1982) and Thorpe (1982).

We note here that in figure 6 of Ivey & Corcos (1982), there is a large asymmetry in the reported density profiles above and below the centreline in the tank, where the pynocline was originally located. The mid-depth density has the value 1.005, while the fluid on the floor has density 1.010 and the fluid at the top has density 0.9975. The reason for this asymmetry is not clear, but mixing asymmetries between the bottom corner with the rigid floor and the top corner with the free upper surface may

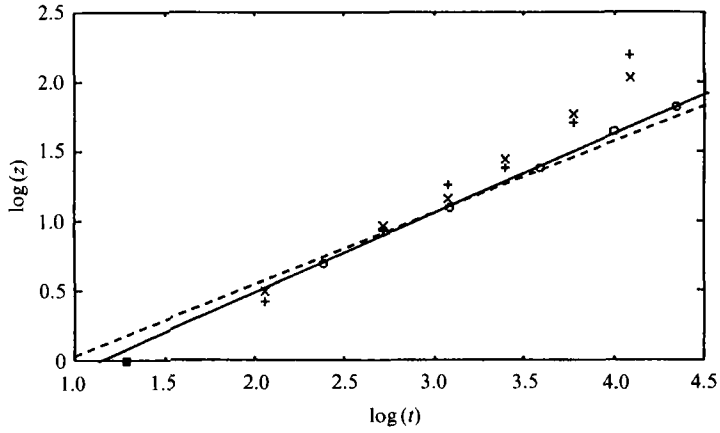

FIGURE 7. Plot of the rate of spread of a pynocline (log (z) *vs.* log (t)) using the data given by Ivey & Corcos (1982) (shown as + and ×) compared with the solid line $z \sim t^{\frac{1}{3}}$, which is the similarity solution of the new theory and the dashed line $z \sim t^{\frac{1}{2}}$, which represents the purely diffusive solution. Also, the points ○ represent values taken from the numerical solution of the advection–diffusion equation which is plotted in figure 6(*b*) for $\rho = 0.3$. These points lie on the solid line showing that the effect of the upper and lower boundaries is small. The theory (solid line) agrees well with the experimental results of Ivey & Corcos for log (*t*) < 3.0, which corresponds to the early stages of the mixing at points near the pynocline. Beyond this time the anomalous mixing in the corners appears to increase the mixing rate above the theoretical prediction.

explain some of the difference in the rate of mixing in this particular experiment compared with similarity theory.

6. Boundary flow on a slope with a turbulent boundary layer

In this section we analyse the more complex problem of mixing at a sloping boundary above which there is a turbulent boundary layer. This problem may exhibit both the turbulent Phillips–Wunsch flow, including the counterflowing circulation, and the turbulence-driven flow discussed in §§4 and 5.

The boundary-layer circulation may be understood as a consequence of the decrease of the eddy diffusivity away from the wall; if the wall is sloping, the eddy diffusivity has both horizontal and vertical gradients which, when combined, can produce horizontal density gradients even if the ambient fluid has a uniform vertical density gradient.

In a non-uniform density gradient, both the dispersive and the turbulent diffusive mass flux may change with depth. This results in the accumulation or diminution of mass in the boundary layer which produces horizontal density gradients; such horizontal density gradients drive a net volume flux along the boundary, as described in §3. Phillips *et al.* (1986) presented a simple dimensional analysis of this flow regime in which they suggested that the mass transport along the boundary is dominated by the dispersion due to the counterflowing circulation. Garrett (1990) investigated this in more detail, calculating the recirculating flow and the association dispersive mass flux, in the case of a uniform ambient density gradient. He showed that the vertical mass flux in the boundary layer equals the sum of the alongslope diffusive and alongslope dispersive mass fluxes. He introduced a mixing efficiency ratio (*I*) defined as the ratio of the actual vertical mass flux in the boundary layer to the mass flux which would be driven by turbulent diffusion alone if the isopycnals remained horizontal. He found $I \leqslant 1$, so that the effect of the circulation is to reduce the total

mass flux; this is because the alongslope dispersive mass flux is less than the cross-slope turbulent diffusive flux would be with horizontal isopycnals.

In this section, we extend these results, pursuing the approach of §2 by calculating the net volume flux along the boundary. We then derive and investigate the interior mixing equation. If the turbulent dispersive and diffusive mass fluxes are not constant, then a net volume flux is produced along the boundary; however, the counterflowing circulation itself has zero net volume flux (except for the molecular Phillips–Wunsch flow contribution (2.1)).

As in §5, we consider the limit in which the boundary-layer width is narrow compared to the scale over which the ambient density gradient changes, $\delta \ll \rho_z/\rho_{zz} = L$. Using the coordinates of figure 1 and writing $\rho(x, y) = \rho_0(z) + \rho_1(x, y)$ where $z = x\sin\theta + y\cos\theta$, the boundary-layer equations are

$$v\frac{\partial\rho_0}{\partial y} + (\boldsymbol{u}\cdot\boldsymbol{\nabla})\rho_1 = \frac{\partial}{\partial y}\left(\kappa_e\frac{\partial(\rho_0+\rho_1)}{\partial y}\right) + \frac{\partial}{\partial x}\left(\kappa_e\frac{\partial(\rho_0+\rho_1)}{\partial x}\right), \tag{6.1}$$

and

$$g\left(\sin\theta\frac{\partial\rho_1}{\partial x} - \cos\theta\frac{\partial\rho_1}{\partial y}\right) = \rho(0)\frac{\partial^2}{\partial x^2}\left(\nu_e\frac{\partial v}{\partial x}\right). \tag{6.2}$$

Integrating the mass conservation equation (6.1) across the boundary layer, we deduce that

$$\psi(\delta)\sin\theta\rho_{0z}(1+0(\delta)) \sim \sin\theta(\overline{\kappa_e}\sin\theta\delta\rho_{0z})_z + \kappa_m\cos\theta\rho_{0z} - \int \mathrm{d}x(\boldsymbol{u}\cdot\boldsymbol{\nabla})\rho_1 + \int \mathrm{d}x\frac{\partial}{\partial y}\left(\kappa_e\frac{\partial\rho_1}{\partial y}\right), \tag{6.3}$$

where $v = \psi_x$ and $u = -\psi_y$ and $\delta\overline{\kappa}_e = \int \kappa_e\,\mathrm{d}x$. On the right-hand side, the first term represents the flow due to the divergent turbulent mass flux, as described in §5. The second term represents the net transport by the Phillips–Wunsch flow itself. The third term is the volume flux due to the divergence in the dispersive flux along the boundary arising from the counterflowing circulation. It reduces to $(\partial/\partial y)\int_0^\infty \psi_x\rho_1\,\mathrm{d}x$ since there is no slip on the wall and $\rho_1 \to 0$ as $x \to \infty$ (i.e. $x > \delta$). The fourth term represents the volume flux induced by the divergence of the perturbation density gradient along the boundary; this is negligible, if ρ_{0z} varies slowly with depth so that the alongslope perturbation density gradient is small compared to the background density gradient (Garrett 1990).

In (6.1) the alongslope advection balances the cross-slope diffusion at leading order within the boundary layer giving

$$v\frac{\partial\rho_0}{\partial y} \sim \frac{\partial}{\partial x}\left(\kappa_e\frac{\partial\rho}{\partial x}\right). \tag{6.4}$$

This implies that within the boundary layer

$$\psi(x) \sim \frac{\kappa_e}{\rho_{0y}}\frac{\partial\rho}{\partial x} \tag{6.5}$$

and so the dispersion term in (6.3) satisfies

$$\frac{\partial}{\partial y}\int\psi_x\rho_1\,\mathrm{d}x \sim -\frac{\partial}{\partial y}\int\psi\frac{\partial\rho_1}{\partial x}\,\mathrm{d}x \sim -\frac{\partial}{\partial y}\int\frac{\kappa_e}{\partial\rho_0/\partial y}\left(\frac{\partial\rho}{\partial x}\right)\left(\frac{\partial\rho}{\partial x} - \frac{\partial\rho_0}{\partial x}\right)\mathrm{d}x. \tag{6.6}$$

The boundary condition $\rho_{0x} = -\rho_{1x}$ at $x = 0$ suggests the scaling $\rho_{1x} = -\lambda(x)\,\rho_{0x}$ in

the boundary layer where $\lambda = O(1)$. Garrett (1990) noted that $\lambda < 1$ over most of the boundary layer and his figure 6 shows that the effectiveness of the mixing $I < 1$. In fact, since Garrett considered the case of very small θ, the alongslope diffusive flux is negligible compared to the alongslope dispersive flux, and so his ratio I reduces to the ratio of the alongslope dispersive flux to the vertical diffusive flux. Therefore, since $I < 1$,

$$\kappa_{\rm d} = \int \lambda(1-\lambda)\,\kappa_{\rm e}\,{\rm d}x < \int \kappa_{\rm e}\,{\rm d}x = \bar{\kappa}_{\rm e},$$

where $\kappa_{\rm d}$ represents the effective diffusion coefficient in the boundary produced by the turbulent dispersion (in the sense of Taylor 1954). The term representing the volume flux induced by the turbulent dispersion, (6.6), may now be written

$$\frac{\partial}{\partial y}\delta\kappa_{\rm d}\rho_{0z}\frac{\cos^2\theta}{\sin\theta}, \tag{6.7}$$

and so from (3.3) the total return flow in the interior therefore scales as

$$W = \kappa_{\rm m}\frac{A_z}{A} + \frac{1}{A\rho_{0z}}\left(\frac{\rho_{0z}\delta(\bar{\kappa}_{\rm e}\sin^2\theta + \kappa_{\rm d}\cos^2\theta)}{\sin\theta}\right)_z. \tag{6.8}$$

The first term represents the molecular Phillips–Wunsch flow and is negligible.

The advection–diffusion equation for the interior mixing resulting from the boundary-driven flow is

$$\rho_t - \frac{A_z}{A}\left(\frac{\hat{\kappa}\delta\int {\rm d}s}{A\sin\theta}\right)\rho_z = \left(\frac{\hat{\kappa}\delta\int {\rm d}s}{\sin\theta A}\rho_z\right)_z, \tag{6.9}$$

where $\hat{\kappa} = \bar{\kappa}_{\rm e}\sin^2\theta + \kappa_{\rm d}\cos^2\theta$ is a function of the local angle of the slope, $\theta(z)$, assumed to vary on a scale much longer than the boundary-layer width δ. The second term on the left-hand side of (6.9) represents the hypsometric effect caused by the changing cross-sectional area of the basin. Note that $\int {\rm d}s\delta/\sin\theta$ is the area of the boundary layer, $A_{\rm b}$, in any horizontal plane. Interior fluid is only mixed at a rate faster than the interior diffusivity if the interior density gradient is non-uniform and there is a strong turbulence-driven boundary flow.

In order to investigate the mixing of the interior further we need to specify the boundary-layer width and eddy diffusivity. As in §5, the boundary-layer width scales according to the maximum size of an eddy whose timescale is less than that of the internal gravity waves (Hopfinger & Toly 1976; Thorpe 1982). For grid-generated turbulent boundary layers, the eddy diffusivity scales as the grid oscillation frequency, ω, oscillation amplitude, a, and the grid spacing, d, giving $\kappa_{\rm e} \sim \omega a^{\frac{3}{2}}d^{\frac{1}{2}}$ and the boundary-layer width scales as $\delta \sim \delta_0/(-\rho_z)^{\frac{1}{4}} = a^{\frac{3}{4}}d^{\frac{1}{4}}\omega^{\frac{1}{2}}/(-\rho_z)^{\frac{1}{4}}$. This expression does not include the dependence of δ upon θ. The leading-order balance from (6.1) and (6.2) gives

$$v\frac{\partial\rho_0}{\partial y} \sim \kappa_{\rm e}\frac{\partial^2(\rho_0+\rho_1)}{\partial x^2}, \quad g\sin\theta\frac{\partial\rho_1}{\partial x} \sim \rho_0\frac{\partial^2}{\partial x^2}\left(\nu_{\rm e}\frac{\partial v}{\partial x}\right).$$

If we write $\rho_1 = -\lambda(x)\rho_0$, where $\lambda = O(1)$ (Garrett 1990), then we require $\delta^4\lambda \sim (1-\lambda)\,\kappa_{\rm e}(\nu_{\rm e}\rho_0/g)/\sin^2\theta\rho_{0z}$. If we adopt the boundary-layer scale $\delta \sim \delta_0/N^{\frac{1}{2}}\sin^{\frac{1}{2}}\theta$, following Phillips *et al.* (1986) and Garrett (1990), with $N^2 = -(g/\rho_0)\rho_z$, then we require $1-\lambda(x)$ and $\lambda(x)$ to be $O(1)$. If the boundary-layer width scales according to the Hopfinger & Toly scale, $\delta \sim \delta_0/N^{\frac{1}{2}}$, then we require $\lambda \sim 1 - a\sin^2\theta$, where a is a constant, and $\kappa_{\rm d} \sim a\kappa_{\rm e}\sin^2\theta$. The difference between these two scales for δ only

becomes significant for very small wall slopes, θ, when $\sin^{\frac{1}{2}}\theta$ is small. In the range of angles studied by Salmun & Phillips, $7 < \theta < 26$, $\sin^{\frac{1}{2}}\theta$ varies from 0.35 to 0.63. This difference is not significantly greater than the error margins in measuring δ, reported by Phillips *et al.* (1986), and so the exact angular dependence may require further measurement. In the following discussion, we set $\delta = \delta_1 \sin(\theta) N^{\frac{1}{2}}$ where $\delta_1(\theta)$ is independent of N.

The interior mixing equation (6.9) may now be rewritten as

$$\rho_t = \delta_1 \hat{\kappa} \frac{-\int \mathrm{d}s(-\rho_z)^{\frac{3}{4}}_z}{\int \mathrm{d}A}. \tag{6.10}$$

For a surface of revolution of radius $R = z^n$, with $\cot\theta = R_z$, the equation for the mixing reduces to

$$\rho_t = -2\delta_1 \hat{\kappa} \frac{(-\rho_z)^{\frac{3}{4}}_z}{z^n}, \tag{6.11}$$

where $\hat{\kappa} = \hat{\kappa}(R_z)$ while for the two-dimensional mixing in a channel the equation is

$$\rho_t = -\delta_1 \hat{\kappa} \frac{(-\rho_z)^{\frac{3}{4}}_z}{z^n}. \tag{6.12}$$

For $n = 0$ and 1, the slope and hence $\hat{\kappa}$ are constant and (6.11) and (6.12) have the similarity variable $\zeta = zt^{-4/(7+4n)}$, where z is the vertical coordinate. The case of a vertical wall, $n = 0$, was considered in §5. In figure 8(*a*), we have plotted the self-similar density profile for a point source spreading from the apex of a two-dimensional channel ($n = 1$), as given by (6.12). In contrast, in figure 8(*b*) we present the evolution with time of a pycnocline mixing in a two-dimensional channel, subject to zero-mass-flux boundary conditions at the upper and lower surfaces, as governed by (6.12). In this solution, the effect of the vertical asymmetry in the basin shape combined with the upper and lower boundary conditions influence the evolution of the density profile significantly. The effect of the geometry may be seen most clearly by comparison with figure 6(*b*). However these solutions (figure 8*b*) are not applicable to a pycnocline in the initial stage of mixing when $\delta \sim L = \rho_z/\rho_{zz}$; this is a very short time unless the wall is nearly horizontal in which case our theory breaks down and the mixing described by Turner (1979) for a horizontal, oscillating grid applies. We now compare the model with the experimental results of Phillips *et al.* (1986) and Salmun & Phillips (1991).

Phillips *et al.* (1986) and Salmun & Phillips (1991) investigated experimentally and theoretically the mixing of a pynocline on a linearly sloping wall. We first focus upon the earlier work. Phillips *et al.* measured the mass flux through a horizontal surface by calculating the rate at which the mass (of salt) above the surface changed with time. They predicted, in a similar manner to the above theory, and also measured experimentally the scaling for the mass flux at the pycnocline

$$F \sim \delta_0 \hat{\kappa} \frac{\cos^2\theta}{\sin^{\frac{3}{2}}\theta} (-\rho_{0z})^{\frac{3}{4}}; \tag{6.13}$$

the dependence upon the slope angle is derived from their assumption that the dispersive mass flux is dominant and also that $\delta \sim d_0/\sin^2\theta(-\rho_z)^{\frac{1}{4}}$. We have included the diffusive flux in our theory, replacing the term $\hat{\kappa}\cos^2\theta$ with the term $\kappa_\mathrm{d}\cos^2\theta + \bar{\kappa}_\mathrm{e}\sin^2\theta$, in view of the results of Garrett (1990), from which we deduced earlier that the alongslope diffusive mass flux is also important. The scaling (6.3) for F in terms

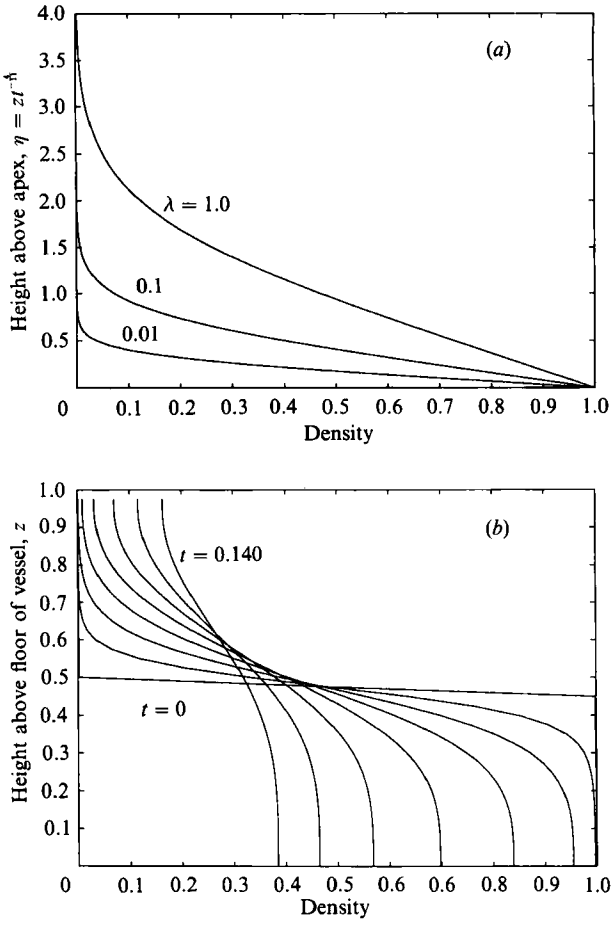

FIGURE 8. (*a*) The similarity solution of (6.12) for the dimensionless density in the interior of the fluid produced by the mixing from the turbulence-driven flow along a linearly sloping boundary, $n = 1$. Solutions are given for $\delta_1 \hat{\kappa} = 1.0$, 0.1 and 0.01. (*b*) The evolution, with time, of a pycnocline spreading in a two-dimensional channel with linearly sloping walls, $n = 1$, as predicted by (6.12), incorporating the effects of the zero-flux conditions at the upper and lower surfaces. Dimensionless density profiles are shown at non-dimensional times 0, 0.005, 0.015, 0.030, 0.050, 0.075, 0.105, 0.140 and $\delta_1 \hat{\kappa} = 1$. The initial condition is shown as the first density profile. The sloping walls change the solution dramatically from that of a vertical wall (figure 6*b*).

of ρ_z is consistent with the results of Ivey & Corcos (1982) and Thorpe (1982), thereby supporting the unifying approach we have presented in this section. Our mixing equation (6.10) suggests that the mass flux F scales as

$$F \sim \delta_1 \frac{\hat{\kappa}(-\rho_{0z})^{\frac{3}{4}}}{L_0 + az}. \tag{6.14}$$

Phillips *et al.* also suggested that the volume flux in the boundary layer had the value (their equation (4.19))

$$F_v = -\frac{A\cos^2\theta(\omega a d)^{\frac{3}{2}} z}{h^2 \sin^{\frac{3}{2}}\theta}\left(\frac{-\rho}{g\rho_{0z}}\right)^{\frac{1}{4}}. \tag{6.15}$$

The similarity solutions of figure 8(*a*) for the mixing of a point source from an apex are not directly applicable to this experiment; only when the mixing front has spread

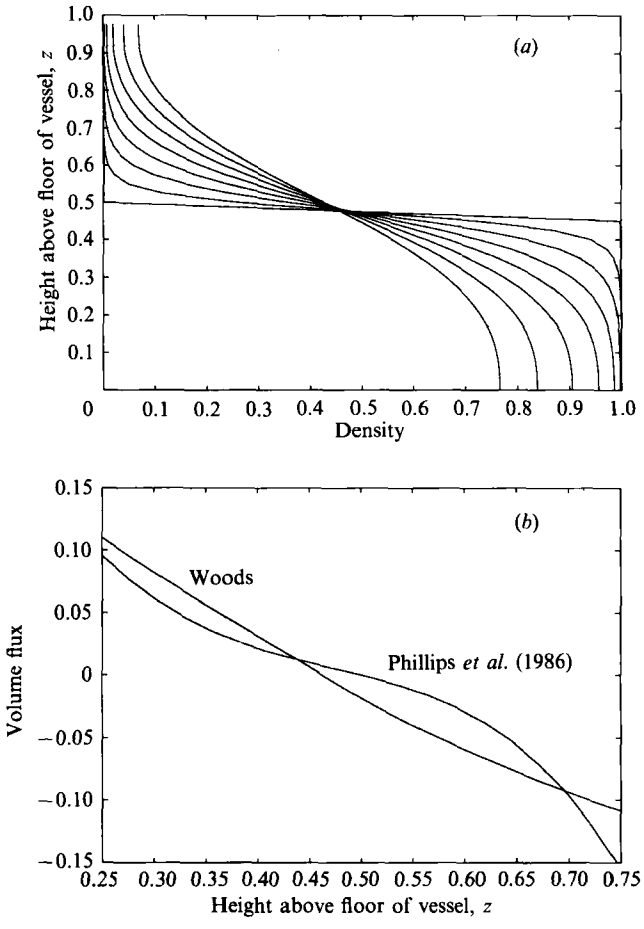

FIGURE 9. (*a*) The evolution with time of a pycnocline spreading in a two-dimensional channel of width $L = \frac{1}{3}+z$, similar to the Phillips *et al.* (1986) experiments. The non-dimensional density field is shown at the non-dimensional times 0, 0.005, 0.015, 0.030, 0.050, 0.075, 0.105, 0.140 and $\delta_1 \hat{\kappa} = 1.0$. Note that the finite width of the channel floor causes the pynocline to spread at a rate intermediate to that of figures 6(*b*) and 8(*b*). (*b*) Comparison of the theoretical volume flux (6.17) predicted by the present theory compared with that given by the scaling of Phillips *et al.* (6.18) at non-dimensional time 0.015, for $\kappa = 1$.

sufficiently far from the apex that $az \gg L_0$ will the mixing asymptote to the similarity solution for $n = 1$ (assuming the mixing process described herein still obtains at that stage). Before this point is reached the interior mixing equation retains some detail about the geometry of the basin and is

$$\rho_t \sim \frac{3\delta_1 \hat{\kappa}(\alpha)\,\rho_{zz}}{4(-\rho_z)^{\frac{1}{3}}(L_0+az)}. \tag{6.16}$$

When $L_0 \geqslant \alpha z$, the mixing will not be self-similar, but will lie between the self-similar vertical-wall mixing rate $z \sim t^{\frac{4}{7}}$ (figure 6) and the self-similar linearly sloping-wall mixing rate $z \sim t^{\frac{4}{11}}$ (figure 8). We have solved (6.16) numerically, starting with a pynocline, using the non-dimensional vessel shape $L = (z+\frac{1}{3})$ where $0 < z < 1$, similar to the experiments of Phillips *et al.* In figure 9(*a*), we have plotted a time sequence of density profiles which is similar to the experimental results of Phillips

et al. Note that at each time the density profiles lie between those of figures 6(*b*) and 8(*b*).

According to our boundary-layer theory the volume flux along the boundary, which is given by (6.8), scales as

$$V_f \sim \frac{-\delta_1 \hat{\kappa} \rho_{0zz}}{(L_0+\alpha z)(-\rho_{0z})^{\frac{5}{4}}}. \tag{6.17}$$

In contrast, Phillips *et al.* argued that the volume flux in the boundary scaled as

$$V_f \sim (z/\kappa t)/(-\rho_{0z})^{\frac{1}{4}} \tag{6.18}$$

(cf. (6.15) with $h \sim (kt)^{\frac{1}{2}}$), based upon the assumption that the density profile remains Gaussian so that $\rho_{0zz}/\rho_{0z} \sim z/(kt)^{\frac{1}{2}}$. In their figure 12, they showed that their experimental data agreed well with (6.18). In figure 9(*b*) we present V_f, as given by (6.17) at the non-dimensional time $t = 0.015$ for $\kappa = 1$. For comparison, we have also plotted expression (6.18), evaluated at $t = 0.015$, scaled such that V_f matches at $z = 0.7$, on figure 9(*b*). There is little difference in the volume flux scaling suggested by Phillips *et al.* (6.18) and that predicted by our boundary-layer theory of the mixing (6.17), particularly near the pynocline, $0.3 < z < 0.7$. This range includes those values of z over which Phillips *et al.* compared (6.18) with their experimental data. Thus we suggest that the expression (6.17) also scales consistently with the experimental data.

As first suggested by Ivey & Corcos (1982), the stream function for the interior flow field is given by

$$\psi_x = -W; \quad \psi_z = W_z(L(z)-x). \tag{6.19}$$

This has solution

$$\psi(x, z) = -Wx + \int L(z)\, W_z \,\mathrm{d}z. \tag{6.20}$$

Salmun & Phillips (1991) recently found experimentally that the mass and volume flux along the boundary increase as the slope angle is increased. This is inconsistent with the scaling that Phillips *et al.* (1986) proposed and which leads to expression (6.13) herein. Using the present boundary-layer theory, we have derived a general expression, (6.14), which includes the mass flux due to both the turbulent diffusion and dispersion. The expression is

$$F = \frac{\delta_1(\bar{\kappa}_e \sin^2\theta + \kappa_d \cos^2\theta)N^{\frac{3}{2}}}{L_0+\alpha z} \tag{6.21}$$

for the mass flux.

As mentioned above, further experimental investigation may be required to establish the precise dependence of δ_1 upon θ. If we adopt the scaling of Phillips *et al.* (1986) for the boundary-layer width, then $\delta_1 \sim \delta_0 \sin^{-\frac{3}{2}}\theta$. In this case, if

$$\bar{\kappa}_e \approx 10^2 \kappa_d \tag{6.22}$$

then expression (6.21) increases with θ for $\theta > 7$ and so is in accord with the experiments of Salmun & Phillips (1991); we note, however, other scalings for δ_1 may also be consistent. The condition (6.22) states that for sufficiently large slope (in this case 7°), the diffusive mass flux exceeds the dispersive mass flux, and therefore the transport can increase with slope angle; Phillips *et al.* did not include the diffusive

transport. Our analysis is consistent with §§4 and 5 in which we showed that when the boundary is vertical, the mass flux is purely diffusive. The condition (6.22) is consistent with, although in the smaller range of, the values of $I \sim \kappa_d/\bar{\kappa}_e$ of Garrett (1990) given in his figure 6. Garrett plotted I as a function of the ratio qh which represents the boundary-layer width divided by the decay scale of the turbulence (which is externally imposed); however his boundary-layer width includes a contribution from the rotation and this increases the value of qh, particularly at small θ. Therefore, in the present non-rotating problem, it may be appropriate to take a value of qh less than unity, in which case it follows from Garrett's figure 6 that $I < 0.4$.

In this section we have combined the boundary-layer flow which is produced by the divergence of both the turbulent diffusive mass flux and the turbulent dispersive mass flux in the sloping boundary layer. We have calculated the interior advection–diffusion equation and identified how the basin shape affects the mixing produced by the turbulence-driven boundary flow. We have shown that the theory is consistent with experiments of mixing on a slope. Similarity solutions exist for mixing at a vertical or linearly sloping wall ($n = 0$ or 1) with similarity variable $\zeta \sim zt^{-4/(7+4n)}$. The rate of mixing caused by such boundary mixing may be compared to the corresponding result with the purely laminar Phillips–Wunsch-driven mixing (§2), in which case the similarity variable has the form $\zeta \sim zt^{-1/(2+n)}$.

7. Application to deep ocean basin mixing

Following Munk (1966), there have been a number of studies aimed at quantifying the mean mixing in the ocean driven by boundary processes. Eriksen (1985), Garrett & Gilbert (1988) and Ivey & Nokes (1989) have addressed the mixing produced by internal waves interacting with sloping walls in order to evaluate the energy which may be available at the wall for mixing. Garrett (1984) and Gregg (1987) analysed the effect of a depth-dependent eddy diffusivity in the interior of the ocean and Ivey (1987*b*) extrapolated his experimental results to the oceanic context following the work of Armi (1978). However, there is still some uncertainty as to the dependence of the eddy diffusion coefficients on the density gradient in the (boundary regions of the) ocean. Therefore, in this section, we assume, purely for simplicity, that $\hat{\kappa}_e \delta$ is a constant. We present a very simple advection–diffusion equation for the mixing of the interior fluid, based upon the present analysis of the boundary-flow-driven mixing. We include an imposed steady source of fluid which produces a mean vertical flow in addition to the boundary-driven, interior return flow. This may be regarded as a very simple model of cold water intruding into the bottom of a deep ocean basin and subsequently being mixed. Owing to the simplicity of the model, we investigate the qualitative effect which the boundary mixing may produce, rather than attempting to simulate a particular oceanic measurement; we have left detailed quantitative application of this model to a further study.

We have ignored the role of rotation, although in some oceanic contexts this may be important. The boundary flows we have described may exist in a rotating system, with a suitable geostrophic zonal flow. However, the rotation may restrict the interior return flow, especially the entrainment and detrainment, to an annulus near the outer boundary, whose width is of the order of the Rossby radius of the system (Ivey 1987*a*). This may then produce spatial inhomogeneities in the interior mixing. In the Appendix, we suggest a simple extension of the bulk, non-rotating boundary-layer theory to include the zonal geostrophic flow which arises in a rotating system;

however such modelling requires further development. This new zonal flow induced by the turbulence-driven boundary flow, has some similarity with the flows of Thorpe (1987) and Garrett (1990) who considered the geostrophic flow arising as a result of the Phillips–Wunsch-type flow in a rotating system.

A volume flux Q input to the floor of the basin will drive a vertical mean flow $Q/\pi R^2$ upwards in the interior of the basin of radius R (ignoring any entrainment which may occur as the input fluid enters the basin over a sill and sinks to the floor). Using the results of §6, the interior mixing is governed by the advection–diffusion equation

$$\rho_t + \frac{Q}{R^2}\rho_z = \frac{2}{R}(\hat{\kappa}_e \delta \rho_z)_z. \tag{7.1}$$

Taking $\delta\hat{\kappa}_e$ to be a constant and $R = L_0 + az$, the steady density profile has the form

$$\rho_z = \rho_{0z}\left(1 + \frac{az}{L_0}\right)^{(Q/2a\hat{\kappa}_e\delta)}. \tag{7.2}$$

With $\rho_{0z} < 0$, the main effect of the input of the cold water is to advect the isopycnals upwards, weakening the density gradients at the base of the vessel and enhancing them at the top. This is consistent with the qualitative form of the density structure in the deep ocean, for example figure 3 of Munk (1966). This density gradient produces an upward boundary flow (cf. §§5, 6) and hence a downward return flow in the basin interior. The density gradient is such that this downward return flow in the fluid interior is equal, but opposite, to the upward flow due to the source of water at the floor of the basin; therefore the net upward flux of water, due to the basal input of water, propagates upwards through the basin via the boundary layer.

In a basin which is long and narrow (e.g. a fjord) the upward flow due to a basal input of cold water may be approximately two-dimensional, of the form Q/L, where Q is the volume flux input per unit length of the channel and L the width of the channel. In this case the advection–diffusion equation becomes

$$\rho_t + \frac{Q}{L}\rho_z = \frac{1}{L}(\hat{\kappa}_e \delta \rho_z)_z. \tag{7.3}$$

Again taking $\hat{\kappa}_e\,\delta$ constant as the simplest model, the steady-state density profile has the form

$$\rho_z = \rho_{0z}\exp\left(\frac{Q(z-z_0)}{\hat{\kappa}_e\delta}\right) \tag{7.4}$$

and the effect of the cold water input is to advect the isopycnals upwards.

In these simple examples, although the mixing is advective it behaves as a diffusive process in which the effective interior diffusivity scales as $(\hat{\kappa}_e\delta\int \mathrm{d}s/\int \mathrm{d}A)$; this is similar to the results of Armi (1978) and Ivey (1987*b*).

8. Conclusion

We have reviewed and quantified the two mechanisms by which a boundary current may be produced in a stratified fluid; (i) the Phillips–Wunsch flow driven by the condition of no normal flux at a sloping wall and (ii) the turbulence-driven flow, produced when there is divergent mass flux in a turbulent boundary layer adjacent to the wall; such a divergent turbulent mass flux is produced when there is either a

non-uniform interior density gradient or a variation in the intensity of the turbulent boundary mixing with height. We have analysed how these different flows mix the fluid interior. The interior mixing equation driven by the laminar Phillips–Wunsch flow is

$$\rho_t = \frac{\kappa(\infty)}{A}(\rho_z A)_z, \tag{8.1}$$

while that produced by a turbulent boundary layer, on a sloping wall, is

$$\rho_t = \frac{1}{A}\left(\rho_z \int \hat{\kappa}\delta \, \mathrm{d}s\right)_z, \tag{8.2}$$

where $\int \delta \, \mathrm{d}s$ is the cross-sectional area of the turbulent boundary layer, A_z the area of the whole basin and $\hat{\kappa} = \bar{\kappa}_e \sin^2\theta + \kappa_d \cos^2\theta$ is the effective vertical eddy diffusivity across the boundary layer which includes both the alongslope turbulent diffusion ($\bar{\kappa}_e \sin^2\theta$) and the alongslope dispersion produced by the counterflowing circulation ($\kappa_d \cos^2\theta$).

The laminar Phillips–Wunsch flow changes the steady-state density profiles in vessels of non-uniform cross-section dramatically in contrast to their linear counterpart in a vertically sided vessel. For example, in a two-dimensional channel with linearly sloping side-walls, the laminar Phillips–Wunsch flow results in a logarithmic steady-state density profile (figure 4).

We have also shown that only through the turbulence-driven boundary flow can the interior mix at a rate significantly different from the purely diffusive value appropriate to the interior. As the slope of the wall increases towards the vertical, the turbulent dispersive mass flux in the boundary layer decreases to zero, and the turbulent diffusive mass flux controls all the boundary-driven mixing. Comparison of figures 6(*b*) and 8(*b*) shows that the manner in which a pynocline adjusts to a uniform density is highly dependent upon the vessel geometry; figure 6(*b*) shows the adjustment in a two-dimensional channel with vertical sidewalls, while in figure 8(*b*) the adjustment occurs in a channel with linearly sloping sidewalls, which meet at an apex. Our model is consistent with published experiments for the mixing at both vertical and sloping sidewalls.

We have investigated the qualitative effect of such mixing in deep ocean basins.

I started this study at the Woods Hole Geophysical Fluid Dynamics Summer Study Program, 1989, and am indebted to many people there and subsequently at Scripps for enlightening discussion, conversation and comments concerning the manuscript. In particular, I would like to thank Professors Larry Armi, Chris Garrett, Glenn Ierley, Jim Ledwell, Owen Phillips, Claes Rooth, Bill Young and two anonymous referees. The author has been supported by the Green Foundation, IGPP, UCSD as a Green Scholar and also the National Science Foundation. Acknowledgement is also due to St John's College, Cambridge for assistance with travel expenses.

Appendix. A simple bulk model of the turbulent boundary flow

The results of §5 suggest a very simple bulk model which describes the turbulence-generated boundary flow. Following the experimental results of Ivey & Corcos (1982), Phillips *et al.* (1986), Salmun & Phillips (1990), Thorpe (1982) and Ivey

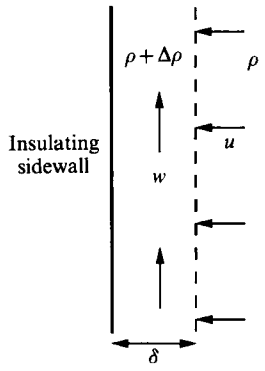

FIGURE 10. Definition of the coordinates for the bulk model of the turbulence-driven boundary flow.

(1987*a*) we deduce that the boundary layer is well mixed and that the time-averaged boundary layer has a sharp interface with the interior, quiescent fluid. For the simple model of this appendix, we assume that the boundary layer has uniform eddy diffusion and viscosity coefficients given by

$$\overline{\nu_e}, \overline{\kappa_e} = \lim(\delta \to 0) \frac{\int_0^\delta \nu_e, \kappa_e(x)\,\mathrm{d}x}{\int_0^\delta \mathrm{d}x}$$

and a uniform vertical velocity $w(z)$, density $\rho_0(z)+\rho_1(z)$, $\rho_1 \ll \rho_0$, and detrainment velocity $u(z)$, with boundary-layer width $\delta(z)$. The bulk equations for the conservation of volume flux, mass flux and momentum flux in the boundary layer, is shown in figure 10, are given by

$$\frac{\mathrm{d}(\delta w)}{\mathrm{d}z} = -u, \tag{A 1}$$

$$\frac{\mathrm{d}(\delta w \rho_0)}{\mathrm{d}z} = \frac{\mathrm{d}}{\mathrm{d}z}\left(\delta \overline{\kappa_e} \frac{\mathrm{d}\rho_0}{\mathrm{d}z}\right) - u\rho_0 \tag{A 2}$$

and

$$\frac{\mathrm{d}(\delta w^2 \rho_0)}{\mathrm{d}z} = -\rho_1 g \delta. \tag{A 3}$$

From these bulk equations, we deduce that

$$w = \frac{(\delta \rho_z \overline{\kappa_e})_z}{\delta \rho_z}; \quad u = -\left[\frac{(\delta \rho_z \overline{k_e})_z}{\rho_z}\right]_z; \quad \rho_1 = \frac{(\delta w^2 \rho)_z}{g\delta}. \tag{A 4}$$

These results are similar to those presented by McDougall (1989); however, he does not consider the subsequent interior mixing. The interior return flow

$$W = \frac{\int \mathrm{d}s}{\int \mathrm{d}A} \frac{(\delta \rho_z \overline{k_e})_z}{\rho_z}. \tag{A 5}$$

From this return flow we deduce that the interior mixing equation has the form

$$\rho_t = \kappa(\infty)\rho_{zz} + \frac{\int \mathrm{d}s(\delta\rho_z \overline{k_e})_z}{\int \mathrm{d}A}. \tag{A 6}$$

This model contains the key physical ingredients for the flow, but is much simpler to analyse. The flow it predicts is identical to the boundary-layer-averaged flow given by the local boundary-layer equations in §5.

A.1. *The effect of rotation*

We may generalize the above bulk boundary-layer analysis to include rotation. We focus upon the boundary-layer dynamics and assume that a suitable interior lateral flow may develop to supply the boundary layer. This assumption merits further investigation owing to the constraints imposed by rotation, although Ivey (1987) reported that in his experiments on boundary mixing in a rotating vessel, the vertical mass flux was mainly effected in the boundary layer. Integrating the boundary-layer equations and assuming azimuthal symmetry, we have

$$\frac{\partial(\delta w)}{\partial z} = -u, \tag{A 7}$$

$$\frac{\partial(\delta w^2)}{\partial z} = \cos\theta f v\delta - g\frac{\rho_1}{\rho_0}\delta\sin\theta, \tag{A 8}$$

$$\frac{\partial(\Delta v w)}{\partial z} = -\cos\theta f w\delta, \tag{A 9}$$

and

$$\frac{\partial(w\delta\rho_0)}{\partial z} = \frac{\partial}{\partial z}\left(\kappa\delta\frac{\partial\rho_0}{\partial z}\right) - u\rho_0, \tag{A 10}$$

where $w(z)$ is the velocity (distance) up the slope, $u(x)$ is the velocity (distance) perpendicular to the slope and $v(y)$ is the velocity (distance) alongslope. Therefore, in addition to the upslope flow

$$w = (\kappa\delta\rho_z)_z/\delta\rho_z \tag{A 11}$$

the rotation induces a zonal flow along the slope v given by

$$v = \frac{1}{f\cos\theta\delta}\left(-wu + \delta w\frac{\partial w}{\partial z} + g\frac{\rho_1}{\rho_0}\delta\sin\theta\right) \tag{A 12}$$

where u is determined by (A 7), (A 10), (A 11).

REFERENCES

Armi, L. 1978 Some evidence for boundary mixing on the deep ocean. *J. Geophys. Res.* **83**, 1971–1979.

Eriksen, C. C. 1985 Implications of ocean bottom reflection for internal wave spectra and mixing. *J. Phys. Oceanogr.* **15**, 1145–1156.

Gargett, A. E. 1984 Vertical eddy diffusivity in the ocean interior. *J. Mar. Res.* **42**, 359–393.

Garrett, C. 1990 The role of secondary circulation in boundary driven mixing. *J. Geophys Res.* **95**, 3181–3188.

GARRETT, C. & GILBERT, D. 1988 Estimates of vertical mixing by internal waves reflected off a sloping bottom. In *Small Scale Turbulence and Mixing in the Ocean, Proc. 19th Intl Liege Colloq. on Ocean Hydrodynamics* (ed. J. J. Nihoul & B. M. Jamart), pp. 405–424. Elsevier.

GREGG, M. C. 1987 Diapycnal mixing in the thermocline – a review. *J. Geophys. Res.* **92**, 5249–5286.

HOPFINGER, E. J. & TOLY, J.-A. 1976 Spatially decaying turbulence and its relation to mixing across density interfaces. *J. Fluid Mech.* **78**, 155–175.

ITSWEIRE, E. C., HELLAND, K. N. & VAN ATTA, C. W. 1986 The evolution of grid-generated turbulence in a stably stratified fluid. *J. Fluid Mech.* **162**, 299–338.

IVEY, G. N. 1987*a* Boundary mixing in a rotating stratified fluid. *J. Fluid Mech.* **183**, 25–44.

IVEY, G. N. 1987*b* The role of boundary mixing in the deep ocean. *J. Geophys. Res.* **92**, 11873–11878.

IVEY, G. N. & CORCOS, G. M. 1982 Boundary mixing in a stratified fluid. *J. Fluid Mech.* **121**, 1–26.

IVEY, G. N. & NOKES, R. I. 1989 Vertical mixing due to the breaking of critical internal waves on sloping boundaries. *J. Fluid Mech.* **204**, 479–500.

KERR, O. 1989 Heating a salinity gradient from a vertical sidewall – linear theory. *J. Fluid Mech.* **207**, 323–352.

LEDWELL, J. R., WATSON, A. J. & BROECKER, W. S. 1986 A deliberate tracer experiment in Santa Monica Basin. *Nature* **322**, 321–323.

MCDOUGALL, T. 1989 Dianeutral mixing. *Aha Huliko Hawaii Winter Workshop Proc.* Hawaii Institute of Geophysics Special Publication.

MUNK, W. H. 1966 Abyssal recipes. *Deep-Sea Res.* **13**, 707–730.

NIR, A. & ACRIVOS, A. 1990 Sedimentation and sediment flow on an inclined plane. *J. Fluid Mech.* **212**, 139–154.

PHILLIPS, O. 1970 On flows induced by diffusion in a stably stratified fluid. *Deep-Sea Res.* **17**, 435–443.

PHILLIPS, O. M., SHYU, J.-H. & SALMUN, H. 1986 An experiment on boundary mixing: mean circulation and transport rates. *J. Fluid Mech.* **173**, 473–499.

SALMUN, H. & PHILLIPS, O. M. 1991 An experiment on boundary mixing. Part 2: Slope dependence and a revised scaling for the boundary layer. *J. Fluid Mech.* (submitted).

TAYLOR, G. T. 1954 The dispersion of matter in turbulent flow through a pipe. *Proc. R. Soc. Lond.* **A223**, 446–468.

THORPE, S. A. 1982 On layers produced by rapidly oscillating a vertical grid in a uniformly stratified fluid. *J. Fluid Mech.* **124**, 391–410.

THORPE, S. A. 1987 Current and temperature variability on the continental slope. *Phil. Trans. R. Soc. Lond.* **A323**, 471–517.

TURNER, J. S. 1979 *Buoyancy Effects in Fluids.* Cambridge University Press.

WUNSCH, C. 1970 On oceanic boundary mixing. *Deep-Sea Res.* **17**, 293–301.